Suppression of Concentration Quenching in Ortho-Substituted Thermally Activated Delayed Fluorescence (TADF) Emitters

Hadi Abroshan, Eunkyung Cho, Veaceslav Coropceanu,* and Jean-Luc Brédas*

School of Chemistry and Biochemistry

Center for Organic Photonics and Electronics

Georgia Institute of Technology

Atlanta, Georgia 30332-0400

*Emails: coropceanu@gatech.edu (V.C.); jean-luc.bredas@chemistry.gatech.edu (J-L.B.)

ABSTRACT

Thermally activated delayed fluorescence (TADF) emitters are typically embedded at low concentrations in a host matrix to suppress emission quenching. However, recent studies indicate that TADF compounds such as the oBFCzTrz emitter display insignificant concentration quenching dependence. To understand the origin of this beneficial behavior, here, the morphology, dynamics, and electronic properties as well as charge transport and energy transfer in a neat film of the oBFCzTrz emitter are characterized via molecular dynamics simulations combined with density functional theory calculations. The emissive layer is found to be in a glassy state at room temperature with the twisted configurations of the emitter molecules allowing for *intra*-molecular donor-acceptor interactions, but disfavoring *inter*-molecular π–π stacking, which suppresses the formation of *inter*-molecular aggregate states. As a result, the electronic structure and luminescence of oBFCzTrz are not significantly altered by *inter*-molecular interactions. The diffusion lengths of the singlet and triplet excitons are calculated to be small enough that there occurs no substantial concentration quenching effect. Overall, the design of new TADF emitters with structural motifs similar to that of oBFCzTrz offers potential to develop efficient OLED devices in which the emissive layers are entirely composed of TADF molecules without the need for a host component.

Keywords: OLED, TADF, morphology, concentration quenching, energy transfer

1. Introduction

Organic materials showing thermally activated delayed fluorescence (TADF) have emerged as a promising class of emitters to promote internal quantum efficiencies (IQEs) of electroluminescence beyond the spin statistical bottleneck of 25%.[1-3] Recent developments in TADF-based organic light-emitting diodes (OLEDs) with an IQE of up to 100% have shifted the material design paradigm of OLEDs from heavy-metal containing phosphors to cost-effective all-organic emitters.[4-11] TADF emitters benefit from the conversion of nonradiative triplet states to the emissive singlet through a reverse intersystem crossing (RISC) mechanism.[1, 12, 13] For an efficient RISC transition, a separation energy (ΔE_{ST}) between the lowest singlet state (S_1) and triplet state (T_1) smaller than 0.2 eV is usually required.[1, 14] To achieve such small ΔE_{ST} values, molecules consisting of donor and acceptor moieties are considered and a precise linkage between them is used to reduce the electronic exchange interactions via formation of twisted donor-acceptor conformations.[15-19] Recently developed TADF systems made of an acceptor such as triazine,[8, 20-27] benzophenone,[28, 29] or diphenylsulfone[3, 30, 31] coupled with a donor like an acridane[25, 30] or carbazole[9, 22, 27, 28, 32] derivative have small ΔE_{ST}, high photoluminescence quantum yield (PLQY), and short delayed fluorescence lifetimes.

TADF emitters are typically embedded at low concentrations (< 20 wt. %) in a host matrix through host–guest co-evaporation in order to suppress emission quenching and/or exciton annihilation due to molecular aggregation.[27, 33, 34] However, recent studies indicate that some TADF emitters can show insignificant concentration quenching dependence, opening a new avenue to simplify OLED structure/fabrication and reduce device manufacturing costs.[5, 25, 35-38] For instance, OLEDs where the active layer has a high concentration of oBFCzTrz (5-(2-(4,6-

diphenyl-1,3,5-triazin-2-yl)phenyl)-5H-benzofuro[3,2-c]carbazole), a blue TADF emitter formed by *ortho*-linkage of benzofurocarbazole to triazine (see Figure 1a), was shown to exhibit high external quantum efficiency (EQE) with low roll-off during operation.[39] Emissive films composed of 8 and 100 wt% of oBFCzTrz showed EQEs of 20.3 and 12.3% at 10 cd/m^2, respectively;[39] the same films displayed EQEs of 12.6 and 13.7% at 1000 cd/m^2, which points to ambipolar transport and, importantly, very limited concentration quenching.[39]

It was suggested that π–π stacking between neighboring molecules could be inhibited via steric hindrance from side chains, thereby minimizing concentration quenching.[40-42] Alternatively, bulky TADF emitters can be employed to reduce the short-range interactions among emitters and suppress quenching.[43, 44] However, the structure of oBFCzTrz and its lack of side chains introduces short-range *inter*-molecular interactions among emitters, making the absence of concentration quenching in neat oBFCzTrz films *a priori* unexpected. In order to provide a molecular insight into the emissive properties of oBFCzTrz neat films, we use an approach that combines molecular dynamics (MD) simulations and density functional theory (DFT) calculations to examine the electronic structure, intersystem crossing transitions, and charge-transport and energy-transfer characteristics in neat oBFCzTrz films.

2. Results and Discussion

2.1. Morphology

The packing configuration of the emissive layer has a strong impact on the optical, energy-transfer, and charge-transport properties and consequently on device performance.[45, 46] In order to obtain an in-depth understanding of the oBFCzTrz neat-film morphology and structural

dynamics, we rely here on atomistic molecular dynamics (MD) simulations. The MD simulation box is illustrated in Figure 1b and the details of the computational approach are given in the Methodology Section. The derived evolutions of the average mean-square-displacements (MSDs) of the center-of-mass (COM) positions of the oBFCzTrz molecules are plotted as a function of MD simulation time (t) in Figures 1c and 1d. At very short simulation times (t < 1 ps), the molecular motions fall into a "ballistic diffusive regime", *i.e.* MSD(t) $\propto t^2$ (Figure 1c), that is dominated by inertia of the emitters and their surroundings.[47] The small magnitude of converged MSD for such a diffusion points to the short distances ($\sqrt{\text{MSD}} \sim$ 0.7 Å) that oBFCzTrz molecules can move in a straight line at a constant velocity before collisions with their surroundings, demonstrating the high local concentration of the film. At longer time scales, the emitters start to move within the instantaneous cages formed by neighboring molecules. Figure 1c indicates that such a "caging diffusive regime" governs the whole simulation time at 300 K; therefore, no appreciable changes in the morphology of the emissive layer occur and the film presents a glassy behavior. What this implies is that, if the system at 300 K is initially located at a local minimum of the energy landscape, it does not have enough thermal energy to jump over energy barriers of local minima to find the global minimum on the potential energy surface.

Next, we carried out MD simulations of the system at higher temperatures, which are close to that used during device fabrication.[39] As temperature increases to 500 and 550 K, the molecules now possess enough thermal energy to "melt" the cages and transit to a diffusive regime, in which case MSD(t) $\propto t$ (see Figure 1d); in these instances, the system can explore the energy landscape and reach the global minimum (generally, the most ordered configuration) in the

course of the annealing procedure. At these higher temperatures, the caging regime that separates the short-time ballistic and long-time diffusive regimes becomes negligible. As the system is then cooled down to room temperature, the dynamics of the oBFCzTrz molecules again become reminiscent of those seen for typical glassy materials, with memory of the initial configuration persisting to a large extent throughout the simulation. This result highlights the importance of the experimental protocols in the preparation of emissive layers since previous studies have shown that thermal annealing strongly influences device performance.[48, 49]

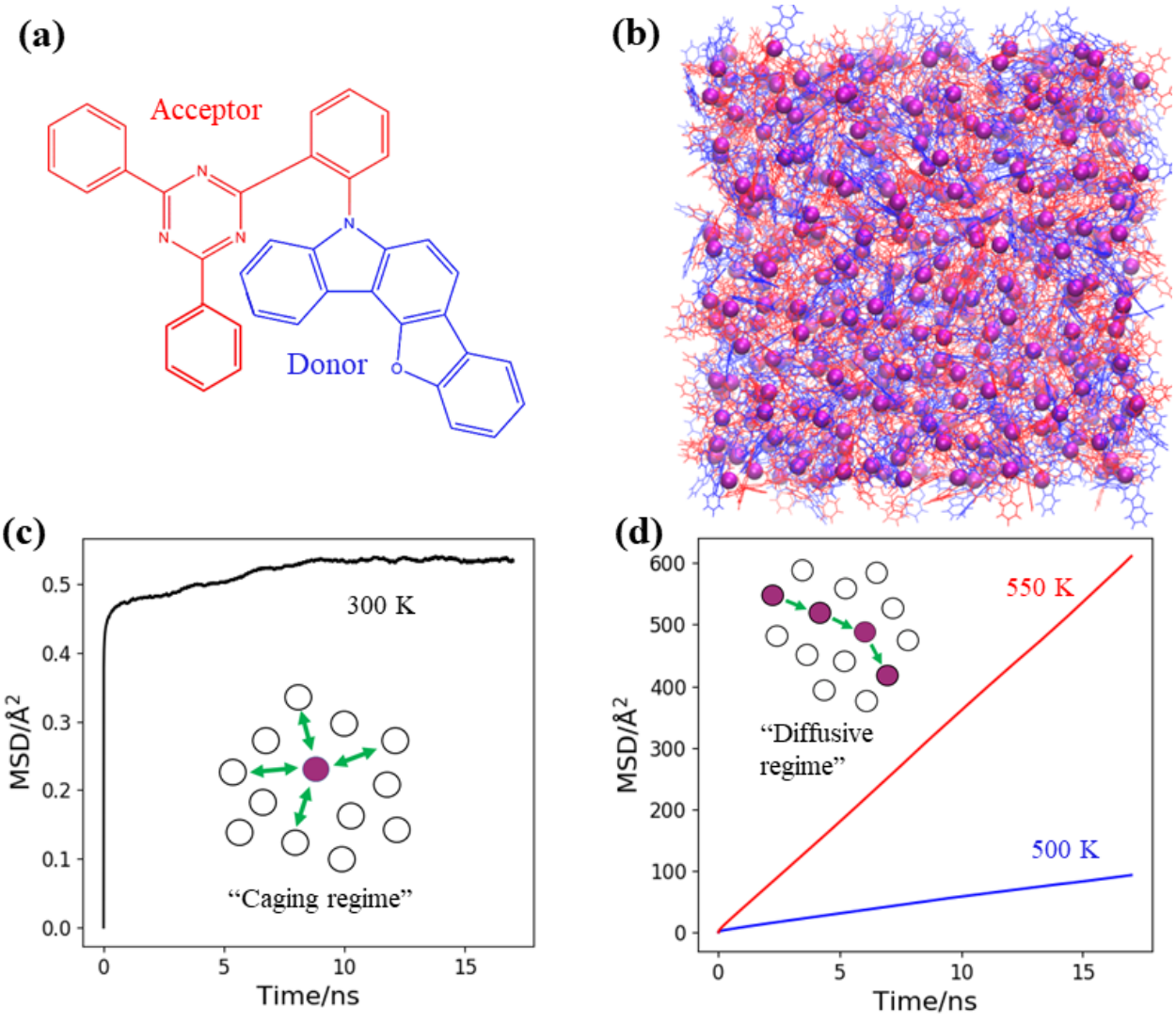

Figure 1. (a) Chemical structure of oBFCzTrz consisting of a donor (benzofurocarbazole) and an acceptor (triazine) moiety. (b) Illustration of the MD simulation cell containing 400 oBFCzTrz molecules. The donor, acceptor, and center of mass (COM) of each molecule are shown in blue, red, and magenta, respectively. Mean-square-displacements (MSDs) of the COMs as a function of simulation time at: (c) 300 K and (d) 500 and 550 K.

The radial distribution functions (RDFs) of the centers-of-mass (COM) of the oBFCzTrz molecules are shown in Figure 2a (we recall that the RDFs correspond to the probability of finding a COM at a distance (R) from another tagged COM). In comparison to the 500 and 550 K cases, the RDF profile at 300 K shows more features owing to the restricted motions of the individual molecules trapped in the cages. As temperature increases to 500 and 550 K, the RDF profile resembles that of a typical fluid whose particles are able to escape from the cages and reach a diffusive regime. At all the temperatures considered here, the RDFs of the system show a general outline where the peak maximum and the first shell boundary are located at around 10.0 and 15.0 Å, respectively.

We evaluated the average number of neighbors around a given molecule as a function of COM separation distance (R). For the sake of accuracy, the number of neighbors is computed directly by using the MD snapshots. Results at 300 K indicate that on average a nearest neighbor molecule is located at $R \sim 8.0$ Å, and the number of neighbors within the first shell ($R \leq 15$ Å) is about 17. At the higher temperatures, the values remain similar. Figures 2b and 2c (black, blue, and red lines) present the RDFs between the COMs of the donor (D) and acceptor (A) molecular subunits (we note that in these RDF calculations of COM_A—COM_D, the donor-acceptor pairs are omitted if both moieties belong to the same molecule). The peak located at ~ 4.1 Å is ascribed to co-facial geometrical D/D, A/A, and D/A configurations, which is confirmed by visual inspection of molecules from the MD snapshots. For the system at 300 K, the occurrence of a

D/A co-facial configuration is found to be slightly larger (~ 31%) in comparison to those of D/D and A/A counterparts. This can be attributed to electrostatic interactions that favor such D/A co-facial configurations. However, a temperature increase to 500 – 550 K leads to equal sampling of all possible pairs (Figure 2c). The RDFs between all the donor and acceptor subunits, including as well those belonging to the same molecule, are also given in Figures 2b and 2c (green line); the results imply that the *intra*-molecular distance between the D and A moieties is about ~ 5.9 Å. Of note, due to the twisted structure of the emitter imposed by the *ortho*-linkage of the D/A moieties, the RDF peak intensity for the *inter*-molecular D/A (~ 4.1 Å) is significantly reduced, *i.e.*, the twisted structure imposes steric hindrance on the *inter*-molecular D/A interactions.

In what follows, we consider the electronic properties of oBFCzTrz at the DFT-optimized geometry as well as within the thin film in the forms of monomers, dimers, and trimers that are extracted from our MD simulations trajectories at 300 K. The results discussed below underline that the aforementioned twisted structure of the oBFCzTrz molecules plays a critical role in minimizing the impact of molecular aggregation on the electronic properties of the emitter in the emissive layer.

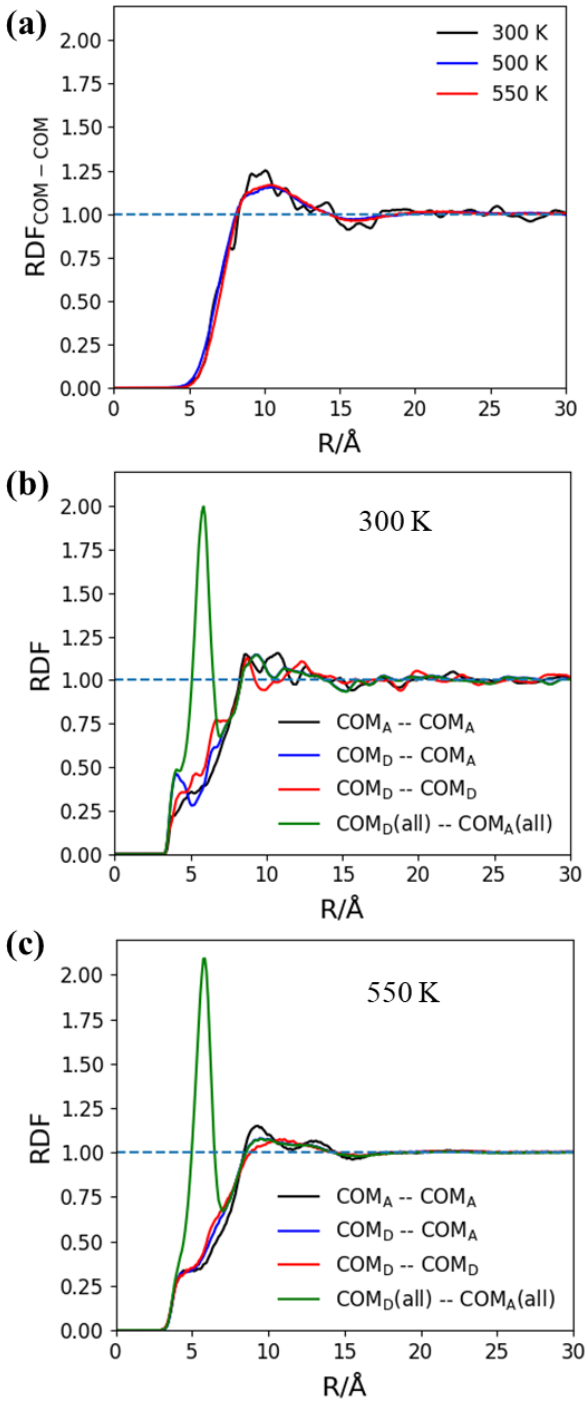

Figure 2. (a) Radial distribution functions (RDFs) between COMs of individual oBFCzTrz molecules (shown as magenta balls in Figure 1b) at 300, 500, and 550 K as a function of separation distance (R). (b) and (c) RDFs for COMs of donor (D) and acceptor (A) fragments of the system (see Figure 1a) at 300 and 550 K. In (b) and (c), the RDFs between all the donor and acceptor subunits of the system are shown in green. The other RDF plots in (b) and (c) are between the subunits that belong to different molecules.

2.2. *Intra*-molecular electronic excitations

To describe the electronic structure of oBFCzTrz, we carried out long-range corrected density functional theory geometry optimizations of an isolated molecule in its ground state (S_0) at the ω_{PCM}B97XD-DFT level, see Methodology Section). The excited-state calculations and the geometry optimizations of the lowest excited singlet state (S_1) and triplet state (T_1) were carried out by means of time-dependent DFT (TDDFT). The calculated singlet adiabatic energy ($E_{S_1}^{Ad}$, Figure 3a) and singlet-triplet splitting energy (ΔE_{ST}) are 2.49 eV and 10 meV, respectively, to be compared to experimental values of 2.99 eV and 2 meV estimated from the onsets of the absorption spectra in thin film;[27] this suggests that the use of the ω_{PCM}B97XD functional underestimates to some extent the excited-state energies, in line with the results of previous studies.[50, 51] The natural transition orbitals (NTOs) indicate that, in both S_1 and T_1 states, the hole and electron are mainly localized on the oBFCzTrz donor (benzofurocarbazole) and acceptor (triazine) moieties, respectively (Figure 3b). The very limited spatial overlap between the hole-NTO and electron-NTO demonstrates the dominant charge-transfer (CT) character of both excited states.

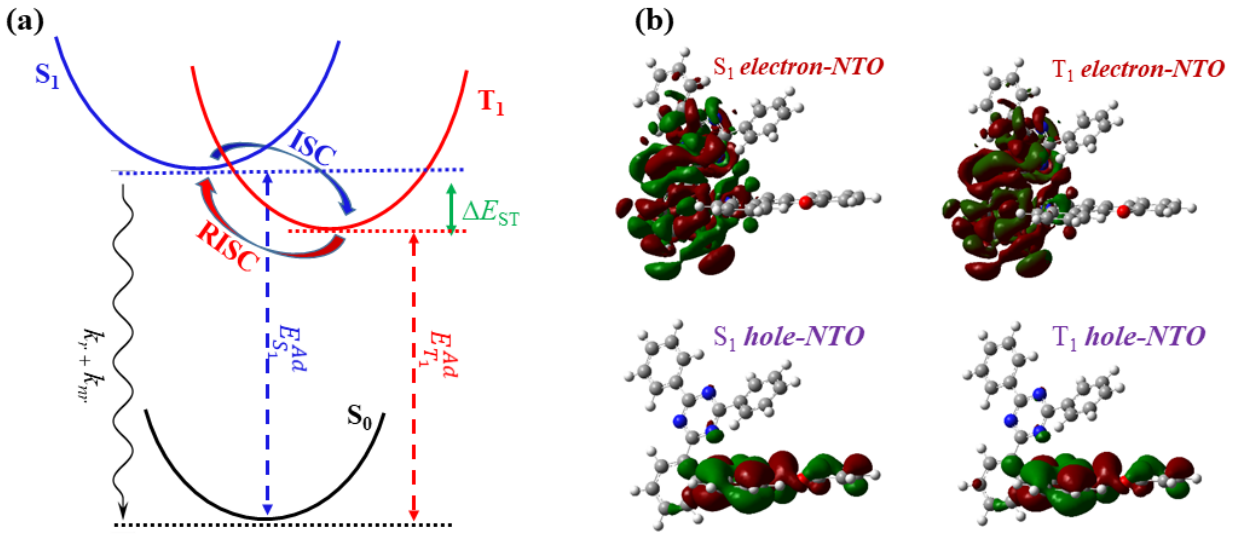

Figure 3. (a) Illustration of intersystem crossing (ISC), reverse intersystem crossing (RISC), singlet adiabatic energy ($E_{S_1}^{Ad}$), triplet adiabatic energy ($E_{T_1}^{Ad}$), rates of radiative and non-radiative decays (k_r & k_{nr}), and singlet-triplet energy separation (ΔE_{ST}). (b) Natural transition orbitals in the S_1 and T_1 states. Atom color code: C, gray; H, white; N, blue; O, red.

Since the molecular geometry in the solid state can be expected to differ from that of the isolated molecule, we randomly extracted 1600 molecules from the MD trajectories, which allows us to account for the effect of molecular packing on the electronic excited-state energies. TDDFT calculations for the selected molecules were then performed to derive the energy distributions of the S_1 and T_1 states. These distributions are Gaussian-like and centered at ~2.86 and ~2.83 eV for S_1 and T_1, respectively, see Figure 4a. The standard deviations (σ) of both S_1 and T_1 energy distributions is ~0.13 eV, which is in good agreement with the value of 0.10 eV estimated from the experimental electroluminescence spectrum of oBFCzTrz.[39] The DFT calculations indicate that the ΔE_{ST} values remain small for the configurational space studied here. As shown in Figure 4b, over 52% of the molecules possess a ΔE_{ST} less than 0.05 eV, ensuring that a considerable ratio of oBFCzTrz monomers can potentially exhibit significant reverse intersystem crossing

rates at room temperature. It is worth mentioning that the ΔE_{ST} values are found to be positive for all the structures considered here; previous studies on TADF emitters have indicated that *inter*-molecular interactions can sometimes alter the relative positions of the S_1 to T_1 states, leading to negative ΔE_{ST} values in the case of a few of the emitters.[52, 53]

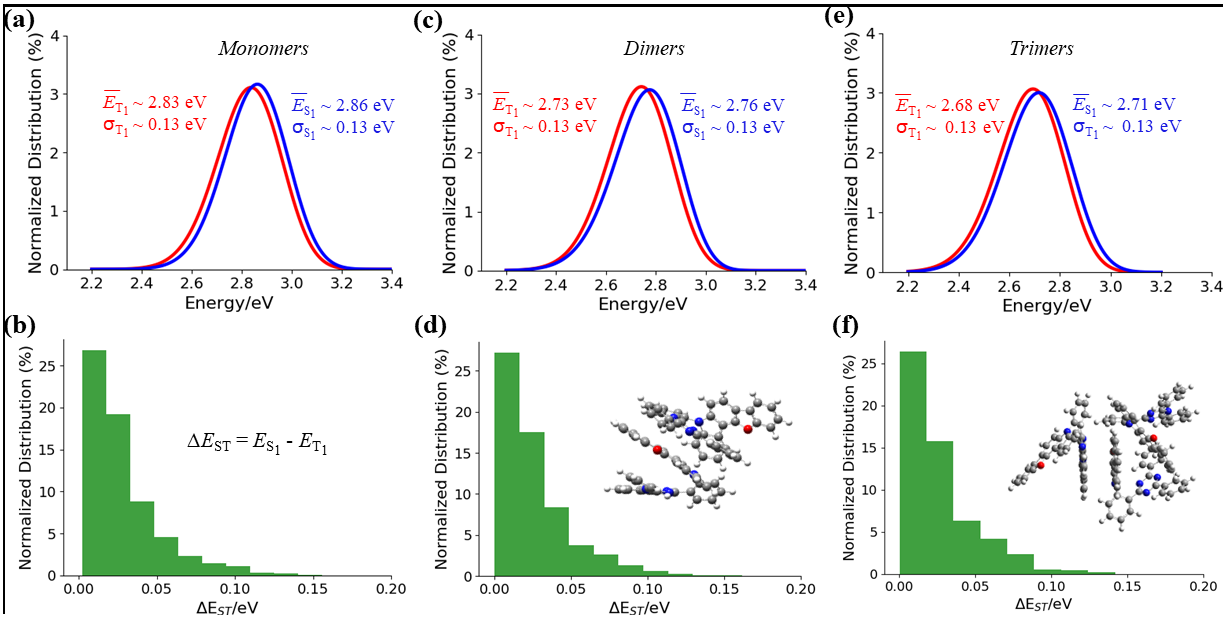

Figure 4. (a), (b) Normalized energy distributions for S_1, T_1, and ΔE_{ST} for 1600 individual molecules of oBFCzTrz extracted from the MD simulations. (c), (d) The same distributions for 1200 dimers, and (e), (f) 500 trimers of oBFCzTrz. Insets in (d) and (e) are random examples of dimers and trimers.

2.3. *Inter*-molecular electronic excitations

Molecular aggregation in an emissive layer can alter the opto-electronic properties of the material[54-58] with the formation of a non-emissive S_1 state being a possible reason for concentration quenching. In order to evaluate the nature of *inter*-molecular states in an oBFCzTrz film, we randomly extracted from the MD simulations 1200 dimers and 500 trimers

of oBFCzTrz where the *inter*-COM distances are within 9.45 Å. Such a distance threshold restricts the sampling of dimers to those where the two interacting monomers are in close vicinity. TDDFT calculations were carried out to estimate the energy distributions of the S_1 and T_1 states for the selected dimers and trimers. The results are illustrated in Figures 4c and 4d, respectively. An NTO analysis shows that the majority of S_1 states are localized on monomers, see Dimer I and Trimer I in Figure 5. However, nearly 10% of the S_1 states in dimers and 13% in trimers have a hybrid character resulting from the mixing of monomer CT and *inter*-molecular CT excitations, see Dimer II and Trimer II in Figure 5. The derived distributions of singlet and triplet states are very similar to those computed for the monomers. As displayed in Figures 4c and 4e, the energy distributions of the lowest excited singlet and triplet states of dimers and trimers are only slightly red-shifted by ~0.10 and ~0.15 eV, respectively, in comparison to those for the monomers (Figure 4a). These results are fully consistent with experimental data pointing to a ~0.11 eV red shift of the emission band in films with a high concentration in oBFCzTrz.[39] The ΔE_{ST} values for dimers and trimers of oBFCzTrz have distribution patterns similar to that of monomers, see Figures 4d and 4f.

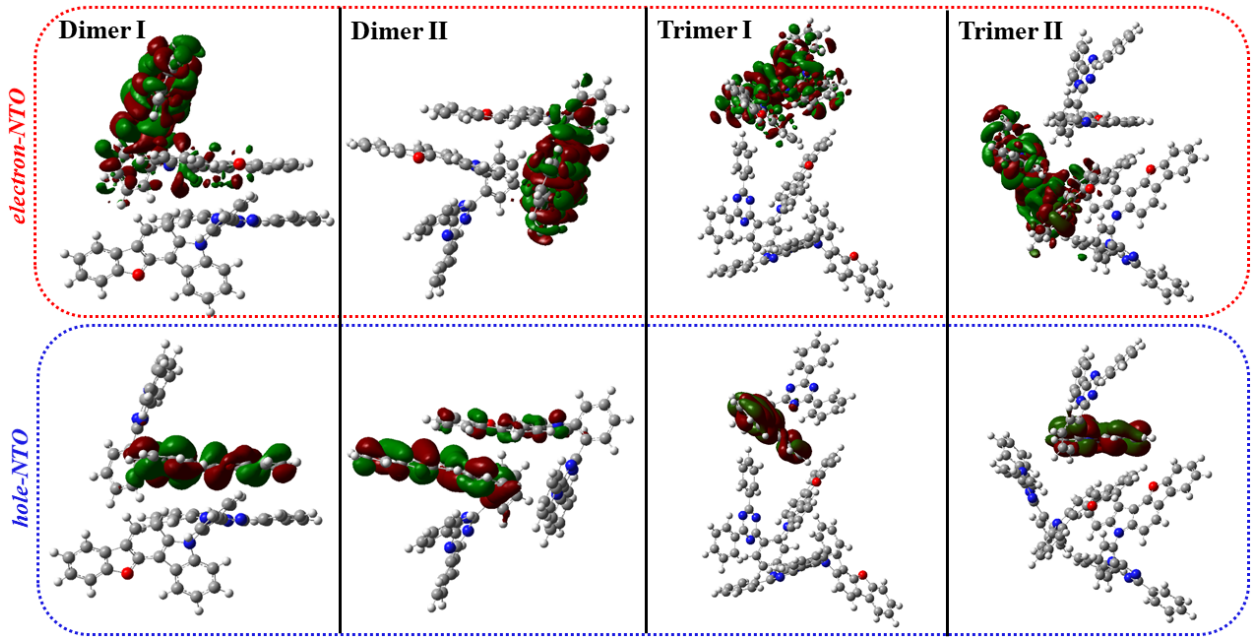

Figure 5. Natural transition orbitals for S_1 in two representative dimers and trimers of oBFCzTrz. Atom color code: C, gray; H, white; N, blue; O, red.

2.4. Radiative transitions

We now turn to the effect of molecular aggregation on the radiative decay rate (k_r) for the electronic transition from S_1 to S_0. These rates were estimated using the Einstein relation[59] (see Methodology Section). They are on the order of 5.10×10^6 s^{-1} for monomers and only very slightly decrease with *inter*-molecular interactions, with values of k_r for dimers and trimers of 4.36×10^6 s^{-1} and 3.55×10^6 s^{-1}, respectively. The photoluminescence quantum yield (PLQY) and the S_1 state lifetime (τ) of oBFCzTrz in thin films are reported to be 82% and 5.4 μs, respectively;[27, 39] these values can be used to approximate the radiative decay rate of the emitter as $\sim \tau \times$ PLQY$= 4.4 \times 10^6$ s^{-1}, which is in excellent agreement with the DFT results. Interestingly, in contrast to the Gaussian distribution displayed by the excited-state energies, the

k_r distribution has an exponential shape (Figure 6a). Further investigations are required to understand the origin behind this feature and its relevance to the device properties.

Overall, our results indicate that aggregation induces only a small red-shift of both singlet and triplet energy distributions and a slight decrease in radiative decay rates, which point to a negligible concentration quenching effect and allow us to rationalize important experimental observations.[39]

2.5. Intersystem crossing transitions

Intersystem crossing is at the heart of the operation of a TADF-based device. The estimation of the ISC and RISC rates (k_{ISC} and k_{RISC}) of the emitter was performed in the framework of Marcus semiclassical electron-transfer model[60] (see Methodology Section). Figure 6b displays the distribution of spin-orbit couplings (V_{SOC}) based on the results obtained for the 1600 oBFCzTrz monomers extracted from the MD simulations. V_{SOC} is calculated to have a mean absolute value of ~0.01 meV (*i.e.*, ~0.1 cm^{-1}), which is on the lower end of the values reported for typical TADF molecules (0.02-0.10 meV).[61] In line with results for other TADF molecules,[53] the V_{SOC} values correlate approximately linearly with the ΔE_{ST} values ($V_{SOC} \propto \Delta E_{ST}$, Figure 7a). This underlines that an increase in V_{SOC} value comes at the expense of an increase in the barrier for the RISC transition. Here as well, further investigations are definitely warranted to gain a better appreciation of the origin of the observed linear relationship between V_{SOC} and ΔE_{ST} in these emitters.

Using V_{SOC} and ΔE_{ST} along with the value of the reorganization energy (see Methodology Section) allows the estimation of the k_{ISC} and k_{RISC} rates (Figures 6c and 6d). The mean values of k_{ISC} and k_{RISC} are 1.22×10^7 s^{-1} and 2.20×10^6 s^{-1}, respectively, which is comparable to those reported for typical TADF emitters.[14, 61] The estimated ISC rate is thus only about 3 times larger than the radiative transition rate; thus, the system is likely to perform only a few cycling transitions between singlet and triplet states before a photon is emitted, which explains the short delayed fluorescence lifetimes observed in oBFCzTrz devices.

We also find a correlation between k_r and k_{RISC}, see Figure 7b, which underlines that the emitter conformations at which the RISC rates are largest often exhibit the lowest radiative decay rates. This correlation points to the fact that the largest values of k_{RISC} are obtained for systems with vanishing ΔE_{ST} values, *i.e.*, for systems that have nearly a pure CT character of the S_1 state and consequently a vanishing oscillator strength for the transition to the ground state (and thus a small k_r). Nevertheless, during the lifetime of the S_1 state, the structural fluctuations due to vibrational dynamics are expected to allow the emitter to sample conformations with higher transition dipole moments and in this way promote radiative decay.

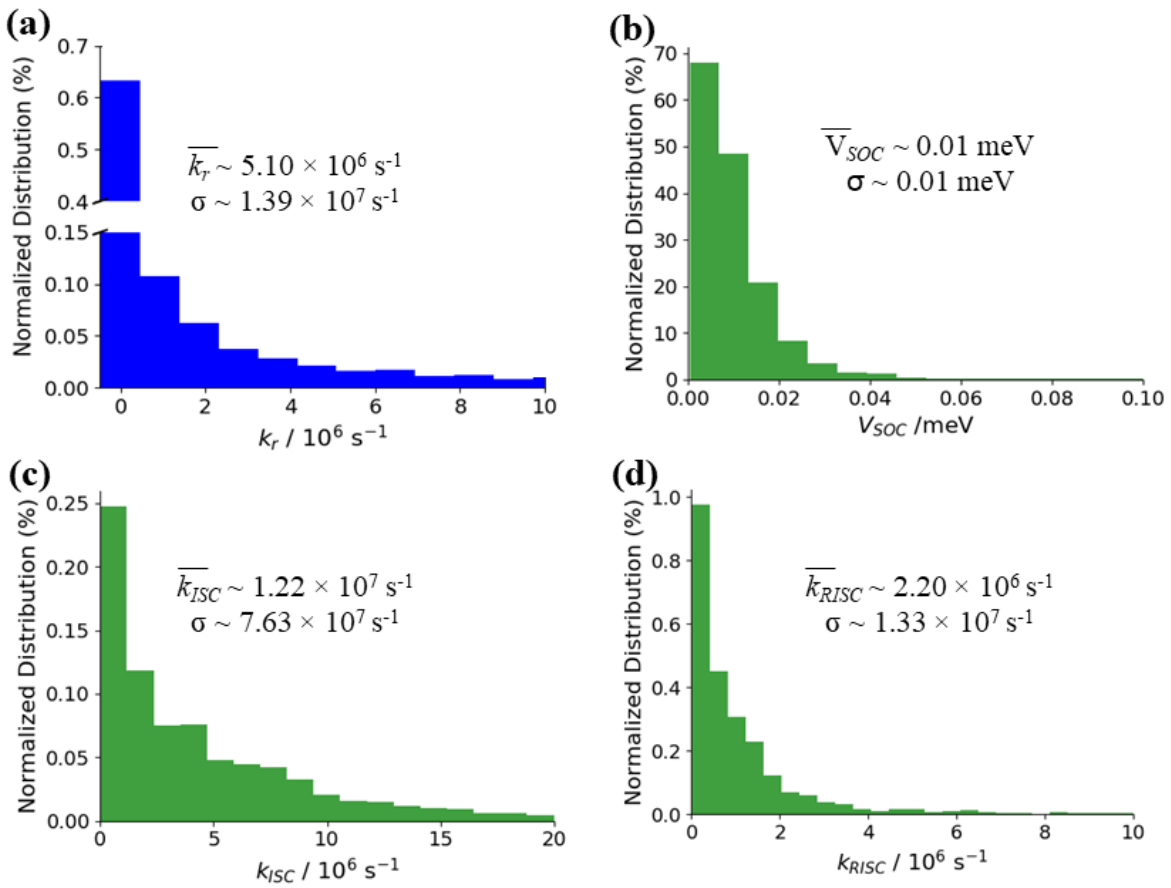

Figure 6. Normalized distributions of (a) spin-orbit couplings (V_{SOC}), (b) intersystem crossing rates (k_{ISC}), and (c) reverse intersystem crossing rates (k_{RISC}) for the 1600 monomers of oBFCzTrz extracted from the MD simulations. (d) Normalized distribution of the radiative decay rates (k_r) for the monomers.

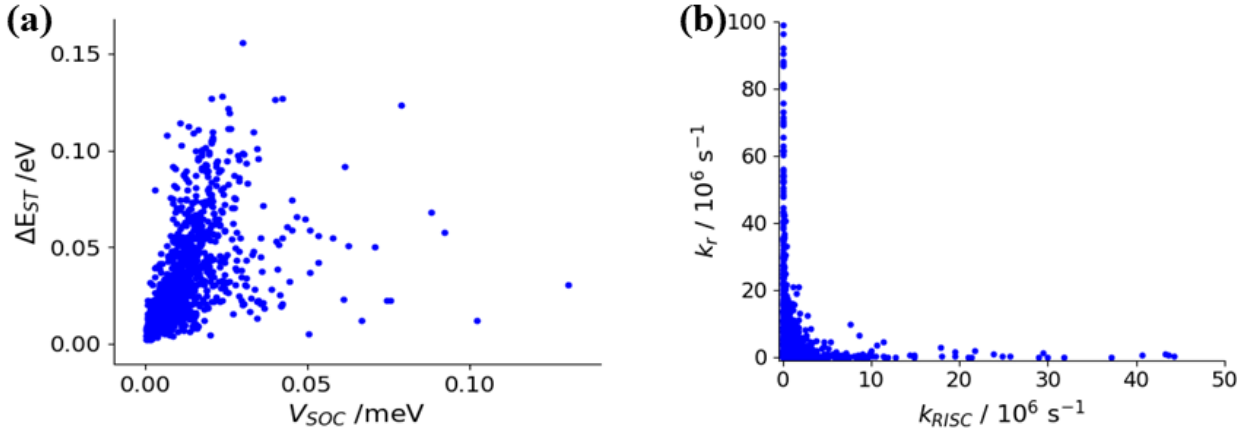

Figure 7. Relationship between (a) ΔE_{ST} and V_{SOC}, and (b) k_{RISC} and k_{ISC} based on the 1600 monomers extracted from the MD simulations.

2.6. Energy transfer

It is also of interest to evaluate the excitation energy transfer (EET) rates among oBFCzTrz molecules. EET processes can lead to non-radiative decay pathways of the excited states via, *e.g.*, exciton-exciton annihilation, which decreases not only the PLQY but also device stability.[62, 63] To evaluate the EET rates, the related electronic couplings were obtained using an approach based on molecular TDDFT transition densities (see Methodology Section).[64, 65] The electronic couplings for the singlet-exciton energy transfer (SEET) processes and triplet-exciton energy transfer (TEET) processes are given in Figure 8a as a function of *inter*-molecular separation distance (R_{COM}), as obtained from calculations performed on the 1600 dimers extracted from the MD snapshots. For dimers composed of monomers in close vicinity (R_{COM} < 9.45), about 96% of the contribution to the electronic coupling for SEET is due to Coulomb interactions, leaving a small portion of about 4% for the contribution related to exchange interactions. For triplet excitons, the Coulomb contribution to the electronic coupling is found to be zero, as expected.

Based on these electronic couplings, the rates for the SEET (k_{SEET}) and TEET (k_{TEET}) processes were calculated; the results are shown in Figure 8b. The k_{SEET} values can be as large as 8.7×10^6 s^{-1} and are about four orders of magnitude larger than the k_{TEET} values, which is mainly due to the higher electronic couplings for SEET than TEET (Figure 8a). Based on the calculated k_{SEET} and k_{TEET} values and considering only energy-transfer processes within a $R_{COM} \leq 0.8$ nm range, the exciton diffusion coefficients (D_L) for the SEET and TEET processes are about 8.74×10^5 and 9.92×10^1 nm^2 s^{-1}, respectively. These diffusion coefficients are significantly lower than those

previously reported for thin films based on conventional organic semiconductors, with $D_{L(SEET)}$ values around 10^{10}-10^{11} nm^2 s^{-1}, and $D_{L(TEET)}$ values around 10^5-10^8 nm^2 s^{-1}.[66-72]

We also evaluated the diffusion length (L_D) for oBFCzTrz excitons within the time, $\tau = 1/k_{RISC}$ = 0.45 μs, that can be considered as the upper limit of the TADF process. The singlet exciton diffusion length is calculated to be ~0.63 nm, which is about one order of magnitude smaller than those found for conventional organic semiconductors such as NPD (N,N′-diphenyl-N,N′-bis(1-naphthyl)-1,1′ biphenyl-4,4″ diamine) (5.1 nm),[73, 74] as well as shorter than the average distance between two oBFCzTrz emitters, ~0.8 nm. As expected, a much smaller diffusion length of about 0.01 nm is derived for triplet excitons. Considering that the exciton density in an OLED based on oBFCzTrz is about 10^{19} cm^{-3} under normal device operation conditions,[39] the average distance between two excitons is evaluated to be about 9.3 nm. Thus, our results suggest that the singlet excitons are able to perform only about one *inter*-molecular hop before decaying to their ground state while the triplet excitons remain essentially immobile during this time. These results underline that the exciton energy-transfer processes in oBFCzTrz films are too slow to lead to any significant luminescence quenching via exciton-exciton annihilation or exciton decay at device interfaces.

In conventional fluorescent emitters and heavy-metal phosphorescent complexes, the Förster[75] mechanism has been found to be the dominant energy transfer mechanism. In contrast, recent concentration quenching measurements[76] performed for xanthone-based TADF emitters suggest a short-range Dexter energy transfer mechanism in these systems.[77, 78] Our results presented above indicate that in oBFCzTrz-based devices the energy transfer mechanism is similar to that

found in conventional OLEDs. However, the rates we have derived are very small, which contributes to a reduction in exciton–exciton annihilation processes and in energy transfer to interfaces and therefore mitigates concentration quenching.

2.7. Charge transport properties

The charge mobility in the emissive layer of OLEDs plays a key role in the formation of excitons and hence in device performance. Thus, we evaluated the electron and hole hopping rates (k_e and k_h) between oBFCzTrz molecules (see Methodology Section), again using 1600 dimers with COM separation distances ≤ 14 Å extracted from the MD simulation trajectories. For each dimer, the electronic couplings between the frontier orbitals of the monomers were calculated and are displayed in Figure 8c. These results were then used as inputs to estimate the charge hopping rates (Figure 8d). We find that the k_h values are two orders of magnitude larger than the k_e values, which suggests that the emission properties in devices based on oBFCzTrz can suffer from a lack of balance between electron and hole mobilities. This result is in agreement with the experimental current-voltage (*J-V*) curves for an oBFCzTrz film,[39] which indicate that the current density is higher for holes than electrons. We note that the larger value of k_h vs. k_e mainly originates in the lower reorganization energy estimated for holes ($\lambda_h \sim 0.19$ eV) vs. electrons ($\lambda_e \sim 0.59$ eV); the greater λ_e value appears to be related to steric effects associated with delocalization of the unpaired electron on both donor and acceptor subunits of oBFCzTrz.

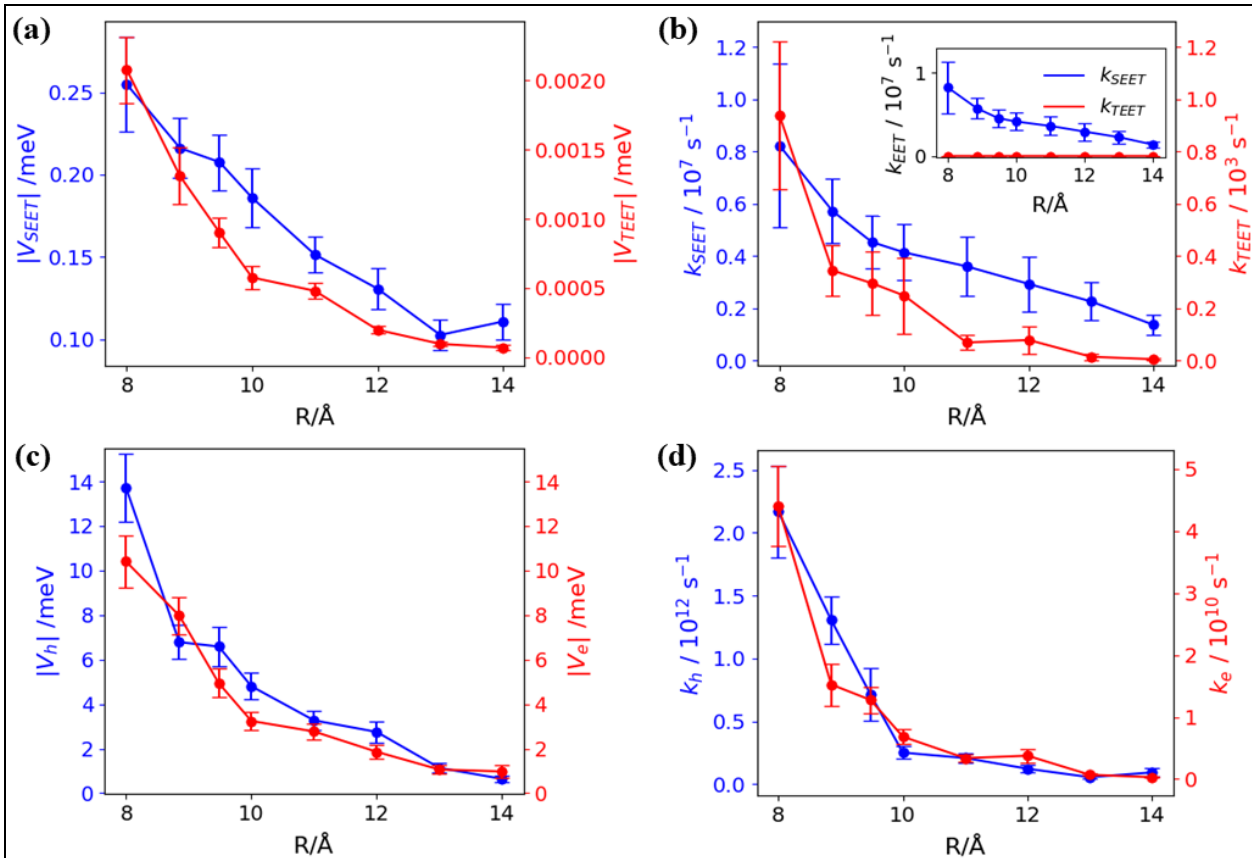

Figure 8. (a), (b) Absolute electronic couplings and rates of excitation-energy transfers for singlet (k_{SEET}) and triplet (k_{TEET}) excitons. (c), (d) Absolute electronic couplings and charge-transport rates for holes ($|V_h|$, k_h) and electrons ($|V_h|$, k_e). The couplings and rates are estimated using 1600 dimers extracted from the MD simulations, as a function of COM separation.

3. Conclusions

We have used a combination of molecular dynamics simulations and density functional theory calculations to study the morphology, structural dynamics, and electronic properties of a neat film of oBFCzTrz, a blue TADF emitter that has been demonstrated to suffer from only very limited concentration quenching in OLED devices. The MD results indicate that a neat film of the emitter presents a "glassy-type" state at 300 K, where the morphology of the film is significantly dependent on the initial packing configuration. The *ortho*-linkage between the

donor and acceptor subunits of the emitter imposes a twisted structures which favors *intra*-molecular noncovalent interactions; a very recent study has shown that these types of interactions enhance spin-orbit couplings between the S_1 and T_1 states, which can significantly improve the reverse inter-system crossing rates.[79] Importantly, the highly twisted structure of the emitter is found to disfavor *inter*-molecular co-facial π–π stacking configurations. As a result, the emitter S_1 and T_1 state energies are hardly influenced by interactions among adjacent emitters in the thin film; these excited states are essentially localized on monomers, which leads to only a small probability of formation of *inter*-molecular CT excitations. These results underline that molecular aggregation minimally impacts the electronic structure of the oBFCzTrz molecules. Thus, the optical properties of the oBFCzTrz molecules are preserved in the emissive layer and remain governed by the highly twisted *intra*-molecular structural motif imposed by the *ortho*-linkage between the donor and acceptor subunits.

The excitation energy-transfer calculations confirm that the Förster mechanism is the dominant pathway of energy transfer among oBFCzTrz molecules. The rates of energy transfer are found to be very small, making exciton-exciton annihilations in the emissive layer unlikely. Combined with the absence of co-facial π-π stacking, this result explains the lack of luminescence quenching in oBFCzTrz neat films.

Overall, our findings highlight that the use of ortho-linked, twisted donor-acceptors motifs can be an efficient design strategy to develop TADF emitters free of concentration quenching effects. However, attention must be paid to the charge-transport properties of this type of emitters, as electron transport in the oBFCzTrz film evaluated here was found to be two orders of magnitude

slower than hole transport, which points to a lack of balance in charge mobility within the active layer, a feature that will require attention in order to improve device operation.

We believe that the multi-tiered simulation and analysis approach of this work can be used as a computational framework to study a wide range of TADF molecules for a systematic design and development of emitters with limited luminescence quenching.

4. Methodology Section

MD Simulations: A 200 × 200 × 200 $Å^3$ cell consisting of 400 oBFCzTrz molecules with a low density of 0.05 g cm^{-3} was initially prepared. An energy minimization and a 5-ns MD simulation using *NPT* ensemble at 1 *atm* and 300 K were first conducted. The resulting system was heated to increase the temperature (*T*) from 300 K to 550 K at 50 K intervals for 1 ns at each temperature. This was followed by an MD simulation with constant *T* at 550 K for 40 ns to allow exploration of the energy landscape. The system thus generated was cooled down from 550 K to 300 K through a 50-ns MD, and next equilibrated for 10 ns. Finally, on the resulting system with cell size of 68.4 × 68.4 × 68.4 $Å^3$ and mass density of 1.17 g cm^{-3}, an MD simulation was carried out for 20 ns to sample the structural characteristics of oBFCzTrz at 300 K. All simulations were performed using the NAMD package.[80] The Langevin dynamics and Nose-Hoover Langevin piston were used to keep the temperature and pressure constant, respectively.[81] To calculate the long-range electrostatic interactions, the particle mesh Ewald (PME) algorithm was employed.[82] The van der Waals forces were truncated using a cutoff of 12 Å, and equations of motion were integrated with a time step of 1 fs. The potential model based on OPLS-AA was used to describe

interactions within the system.[83] Using a protocol developed in our group,[84] the dihedral parameters, equilibrium values of bonds and angles, and the partial atomic charges of the force field for oBFCzTrz were updated using long-range corrected DFT calculations.

DFT Calculations: The Gaussian 09 package was used to perform the calculations using the long-range corrected ωB97XD functional with the 6-31G(d,p) basis set.[85, 86] We optimized the range-separation parameter ω through minimizing $J(\omega)$, defined as $J(\omega) = (E_{HOMO} + IP)^2 + (E_{LUMO} + EA)^2$.[87] The calculations were performed for a molecule embedded in a dielectric medium using the polarizable continuum model (PCM). We employed a dielectric constant (ε) of 3.5, which is a value commonly considered for TADF systems.[88-90] Here, E_{HOMO} and E_{LUMO} denote HOMO and LUMO energies, while IP and EA denote the vertical first ionization potential and electron affinity of the molecule. An optimum ω_{pcm} value of 0.0217 was obtained. The Tamm-Dancoff approximation within time-dependent DFT (TDA-TDDFT)[91-94] was used to estimate the excited-state transition energies and optimize the molecular geometries in the excited states. Previous studies have pointed out that the TDA approach provides a better description of singlet and triplet excitations than TD-DFT.[95, 96]

ISC and RISC Rates: The semiclassical Marcus equation[60] was employed to examine the rates of ISC and RISC (k_{ISC} and k_{RISC}):

$$k = \frac{2\pi}{\hbar} |V|^2 \frac{1}{\sqrt{4\pi k_B T \lambda}} exp\left(-\frac{(\lambda + \Delta E_{ST})^2}{4\lambda k_B T}\right) \quad (1)$$

where, $\hbar$, k_B, and T, denote the reduced Planck constant, the Boltzmann constant, and temperature, respectively. We randomly extracted 1600 structures of the emitter from MD snapshots and calculated the singlet-triplet energy separations ($\Delta E_{ST} = E_{S_1} - E_{T_1}$). Spin-orbit

couplings (V_{SOC}) between S_1 and T_1 were calculated according to the method of linear-response time-dependent density functional using the PySOC and MolSOC codes.[97, 98]

The reorganization energies associated with the ISC and RISC transitions were calculated using the potential energy surfaces (PES) of the related triplet and singlet states as discussed in detail elsewhere.[61]

Radiative Decay Rates: The Einstein equation[59] was used to estimate the radiative decay rate (k_r):

$$k_r = \frac{{E_{S_1}}^3 f(n)}{3\varepsilon_\circ \pi \hbar^4 c^3} \mu^2 \qquad (2)$$

where, $\varepsilon_\circ$, c, E_{S_1}, and μ denote the vacuum permittivity, speed of light, energy of S_1 relative to S_0, and transition dipole moment between the S_0 and S_1 states of the monomers, respectively; $f(n)$ is a function of the refractive index (n) of the emissive layer to account for the local-field effect on the radiative decay. Within the Lorentz virtual cavity model, we considered $f(n) = \frac{n(n^2+2)^2}{9}$,[99] and n = 1.8 for a neat film of oBFCzTrz.

Energy Transfer Rates: To evaluate the rates of excited-state energy transfer, we used the semiclassical Marcus equation (Eq. 1). The electronic couplings for energy transfer between two neighboring A and B molecules (V_{AB}) [100-102] were determined using:

$$V_{AB} = \int dr \int dr' \rho_A^*(r)\, \rho_B(r') \frac{1}{|r - r'|} + \int dr \int dr' \rho_A^*(r)\, \rho_B(r') g_{XC}(r, r', \omega_0) - \omega_0 \int dr \rho_A^*(r)\, \rho_B(r) \quad (3)$$

where ρ_A and ρ_B denote the transition densities of molecules A and B; g_{xc} and ω_0 are the exchange-correlation kernel and transition frequency, respectively. The first and second terms on the right-hand side of Eq. 3 are due to *inter*-molecular Coulomb (Förster coupling) and exchange-correlation (Dexter coupling) interactions, respectively. The last term is the orbital-overlap correction contribution. We randomly extracted 1600 dimer structures from the MD snapshots and calculated the electronic couplings using Gaussian 16.[85] The change in energy due to SEET and TEET processes is approximated as $\Delta E_{SEET} = E_{S_1(A)} - E_{S_1(B)}$ and $\Delta E_{TEET} = E_{T_1(A)} - E_{T_1(B)}$, where $E_{S_1(A)}$, $E_{T_1(A)}$, $E_{S_1(A)}$, and $E_{T_1(A)}$ are the energy of the S_1 and T_1 states for two neighboring molecules A and B. The reorganization energies for the SEET and TEET processes are estimated by means of PES calculations and found to be 0.89 and 0.84 eV, respectively.

The exciton diffusion coefficients were evaluated in the framework of the Smoluchowski–Einstein theory of random walks,[103] as $D_L = \frac{d^2 k}{6}$, where d and k are the distance between the emitters and the hopping rate, respectively. The diffusion length L_D are then calculated as $L_D = \sqrt{D_L \tau}$.[104]

Charge Transport Rates. The semiclassical Marcus equation (Eq. 1) was also used to evaluate the rates of charge hopping between 1600 oBFCzTrz dimers that are randomly extracted from the MD trajectory. The electronic couplings for holes and electron (V_h and V_e) were estimated

through a fragment orbital approach with a basis set orthogonalization procedure.[105] The change in energy due to transfer of an electron (ΔE_e) and hole (ΔE_h) was approximated by calculating the energy difference in LUMOs and HOMOs of neighboring monomers, respectively. The reorganization energies associated with the transfer of holes (λ_h) and electrons (λ_e) were estimated, as in the case of intersystem crossing, by means of PES calculations.

Acknowledgements

This work was funded by the Department of Energy (Award DE-EE 0008205). The authors acknowledge the use of the computing facilities of the Partnership for an Advanced Computing Environment (PACE) at the Georgia Institute of Technology and the support of the PACE team. They are grateful to Kyulux for generous support of their activities.

References.

[1] H. Uoyama, K. Goushi, K. Shizu, H. Nomura and C. Adachi, Highly efficient organic light-emitting diodes from delayed fluorescence, *Nature*, **2012**, *492*, 234.

[2] K. Goushi, K. Yoshida, K. Sato and C. Adachi, Organic light-emitting diodes employing efficient reverse intersystem crossing for triplet-to-singlet state conversion, *Nat. Photonics*, **2012**, *6*, 253.

[3] Q. S. Zhang, J. Li, K. Shizu, S. P. Huang, S. Hirata, H. Miyazaki and C. Adachi, Design of efficient thermally activated delayed fluorescence materials for pure blue organic light emitting diodes, *J. Am. Chem. Soc.*, **2012**, *134*, 14706.

[4] Y. Tao, K. Yuan, T. Chen, P. Xu, H. H. Li, R. F. Chen, C. Zheng, L. Zhang and W. Huang, Thermally activated delayed fluorescence materials towards the breakthrough of organoelectronics, *Adv. Mater.*, **2014**, *26*, 7931.

[5] Q. S. Zhang, D. Tsang, H. Kuwabara, Y. Hatae, B. Li, T. Takahashi, S. Y. Lee, T. Yasuda and C. Adachi, Nearly 100% internal quantum efficiency in undoped electroluminescent devices employing pure organic emitters, *Adv. Mater.*, **2015**, *27*, 2096.

[6] F. B. Dias, K. N. Bourdakos, V. Jankus, K. C. Moss, K. T. Kamtekar, V. Bhalla, J. Santos, M. R. Bryce and A. P. Monkman, Triplet harvesting with 100% efficiency by way of thermally activated delayed fluorescence in charge transfer OLED emitters, *Adv. Mater.*, **2013**, *25*, 3707.

[7] H. Wang, L. Xie, Q. Peng, L. Meng, Y. Wang, Y. Yi and P. Wang, Novel thermally activated delayed fluorescence materials–thioxanthone derivatives and their applications for highly efficient OLEDs, *Adv. Mater.*, **2014**, *26*, 5198.

[8] H. Kaji, H. Suzuki, T. Fukushima, K. Shizu, K. Suzuki, S. Kubo, T. Komino, H. Oiwa, F. Suzuki, A. Wakamiya, Y. Murata and C. Adachi, Purely organic electroluminescent material realizing 100% conversion from electricity to light, *Nat. Commun.*, **2015**, *6*, 8476.

[9] T.-A. Lin, T. Chatterjee, W.-L. Tsai, W.-K. Lee, M.-J. Wu, M. Jiao, K.-C. Pan, C.-L. Yi, C.-L. Chung, K.-T. Wong and C.-C. Wu, Sky-blue organic light emitting diode with 37% external quantum efficiency using thermally activated delayed fluorescence from spiroacridine-triazine hybrid, *Adv. Mater.*, **2016**, *28*, 6976.

[10] D. Zhang, L. Duan, C. Li, Y. Li, H. Li, D. Zhang and Y. Qiu, High-efficiency fluorescent organic light-emitting devices using sensitizing hosts with a small singlet–triplet exchange energy, *Adv. Mater.*, **2014**, *26*, 5050.

[11] B. L. Cotts, D. G. McCarthy, R. Noriega, S. B. Penwell, M. Delor, D. D. Devore, S. Mukhopadhyay, T. S. De Vries and N. S. Ginsberg, Tuning thermally activated delayed fluorescence emitter photophysics through solvation in the solid state, *ACS Energy Lett.*, **2017**, *2*, 1526.

[12] M. K. Etherington, J. Gibson, H. F. Higginbotham, T. J. Penfold and A. P. Monkman, Revealing the spin–vibronic coupling mechanism of thermally activated delayed fluorescence, *Nat. Commun.*, **2016**, *7*, 13680.

[13] F. B. Dias, J. Santos, D. R. Graves, P. Data, R. S. Nobuyasu, M. A. Fox, A. S. Batsanov, T. Palmeira, M. N. Berberan-Santos, M. R. Bryce and A. P. Monkman, The role of local

triplet excited states and D-A relative orientation in thermally activated delayed fluorescence: photophysics and devices, *Adv. Sci.*, **2016**, *3*, 1600080.

[14] T. Hosokai, H. Matsuzaki, H. Nakanotani, K. Tokumaru, T. Tsutsui, A. Furube, K. Nasu, H. Nomura, M. Yahiro and C. Adachi, Evidence and mechanism of efficient thermally activated delayed fluorescence promoted by delocalized excited states, *Sci. Adv.*, **2017**, *3,* e1603282.

[15] M. Y. Wong and E. Zysman-Colman, Purely organic thermally activated delayed fluorescence materials for organic light-emitting diodes, *Adv. Mater.*, **2017**, *29*, 1605444.

[16] S. Schott, E. R. McNellis, C. B. Nielsen, H. Y. Chen, S. Watanabe, H. Tanaka, I. McCulloch, K. Takimiya, J. Sinova and H. Sirringhaus, Tuning the effective spin-orbit coupling in molecular semiconductors, *Nat. Commun.*, **2017**, *8*, 15200.

[17] Y. Olivier, M. Moral, L. Muccioli and J. C. Sancho-Garcia, Dynamic nature of excited states of donor-acceptor TADF materials for OLEDs: how theory can reveal structure-property relationships, *J. Mater. Chem. C*, **2017**, *5*, 5718.

[18] B. Milian-Medina and J. Gierschner, Computational design of low singlet-triplet gap all-organic molecules for OLED application, *Org. Electron.*, **2012**, *13*, 985.

[19] X. K. Chen, D. Kim and J. L. Bredas, Thermally activated delayed fluorescence (TADF) path toward efficient electroluminescence in purely organic materials: molecular level insight, *Acc. Chem Res*, **2018**, *51*, 2215.

[20] M. Kim, S. K. Jeon, S.-H. Hwang and J. Y. Lee, Stable blue thermally activated delayed fluorescent organic light-emitting diodes with three times longer lifetime than phosphorescent organic light-emitting diodes, *Adv. Mater.*, **2015**, *27*, 2515.

[21] D. R. Lee, M. Kim, S. K. Jeon, S. H. Hwang, C. W. Lee and J. Y. Lee, Design strategy for 25% external quantum efficiency in green and blue thermally activated delayed fluorescent devices, *Adv. Mater.*, **2015**, *27*, 5861.

[22] S. Hirata, Y. Sakai, K. Masui, H. Tanaka, S. Y. Lee, H. Nomura, N. Nakamura, M. Yasumatsu, H. Nakanotani, Q. S. Zhang, K. Shizu, H. Miyazaki and C. Adachi, Highly efficient blue electroluminescence based on thermally activated delayed fluorescence, *Nat. Mater.*, **2015**, *14*, 330.

[23] H. Tanaka, K. Shizu, H. Miyazaki and C. Adachi, Efficient green thermally activated delayed fluorescence (TADF) from a phenoxazine-triphenyltriazine (PXZ-TRZ) derivative, *Chem. Commun.*, **2012**, *48*, 11392.

[24] K. Shizu, M. Uejima, H. Nomura, T. Sato, K. Tanaka, H. Kaji and C. Adachi, Enhanced electroluminescence from a thermally activated delayed-fluorescence emitter by suppressing nonradiative decay, *Phys. Rev. Appl.* **2015**, *3*, 014001.

[25] W.-L. Tsai, M.-H. Huang, W.-K. Lee, Y.-J. Hsu, K.-C. Pan, Y.-H. Huang, H.-C. Ting, M. Sarma, Y.-Y. Ho, H.-C. Hu, C.-C. Chen, M.-T. Lee, K.-T. Wong and C.-C. Wu, A versatile thermally activated delayed fluorescence emitter for both highly efficient doped and non-doped organic light emitting devices, *Chem. Commun.* **2015**, *51*, 13662.

[26] M. Kim, S. K. Jeon, S.-H. Hwang, S.-S. Lee, E. Yu and J. Y. Lee, Correlation of molecular structure with photophysical properties and device performances of thermally activated delayed fluorescent emitters, *J. Phys. Chem. C* **2016**, *120*, 2485.

[27] D. R. Lee, J. M. Choi, C. W. Lee and J. Y. Lee, Ideal molecular design of blue thermally activated delayed fluorescent emitter for high efficiency, small singlet–triplet energy splitting, low efficiency roll-off, and long lifetime, *ACS Appl. Mater. Interfaces* **2016**, *8*, 23190.

[28] S. Y. Lee, T. Yasuda, Y. S. Yang, Q. S. Zhang and C. Adachi, Luminous butterflies: efficient exciton harvesting by benzophenone derivatives for full-color delayed fluorescence OLEDs, *Angew. Chem. Int. Edit.* **2014**, *53*, 6402.

[29] P. Rajamalli, N. Senthilkumar, P. Gandeepan, P. Y. Huang, M. J. Huang, C. Z. Ren-Wu, C. Y. Yang, M. J. Chiu, L. K. Chu, H. W. Lin and C. H. Cheng, A new molecular design based on thermally activated delayed fluorescence for highly efficient organic light emitting diodes, *J. Am. Chem. Soc.* **2016**, *138*, 628.

[30] Q. S. Zhang, B. Li, S. P. Huang, H. Nomura, H. Tanaka and C. Adachi, Efficient blue organic light-emitting diodes employing thermally activated delayed fluorescence, *Nat. Photonics* **2014**, *8*, 326.

[31] S. H. Wu, M. Aonuma, Q. S. Zhang, S. P. Huang, T. Nakagawa, K. Kuwabara and C. Adachi, High-efficiency deep-blue organic light-emitting diodes based on a thermally activated delayed fluorescence emitter, *J. Mater. Chem. C* **2014**, *2*, 421.

[32] W. J. Park, Y. Lee, J. Y. Kim, D. W. Yoon, J. Kim, S. H. Chae, H. Kim, G. Lee, S. Shim, J. H. Yang and S. J. Lee, Effective thermally activated delayed fluorescence emitter and its performance in OLED device, *Synth. Met.* **2015**, *209*, 99.

[33] B. S. Kim and J. Y. Lee, Engineering of mixed host for high external quantum efficiency above 25% in green thermally activated delayed fluorescence device, *Adv. Funct. Mater.* **2014**, *24*, 3970.

[34] J. W. Sun, J.-H. Lee, C.-K. Moon, K.-H. Kim, H. Shin and J.-J. Kim, A fluorescent organic light-emitting diode with 30% external quantum efficiency, *Adv. Mater.* **2014**, *26*, 5684.

[35] J. Guo, X.-L. Li, H. Nie, W. Luo, S. Gan, S. Hu, R. Hu, A. Qin, Z. Zhao, S.-J. Su and B. Z. Tang, Achieving high-performance nondoped OLEDs with extremely small efficiency roll-off by combining aggregation-induced emission and thermally activated delayed fluorescence, *Adv. Funct. Mater.* **2017**, *27*, 1606458.

[36] Y. Wada, K. Shizu, S. Kubo, T. Fukushima, T. Miwa, H. Tanaka, C. Adachi and H. Kaji, Highly efficient solution-processed host-free organic light-emitting diodes showing an external quantum efficiency of nearly 18% with a thermally activated delayed fluorescence emitter, *Appl. Phys. Express* **2016**, *9*, 032102.

[37] X. Q. Zhang, M. W. Cooper, Y. D. Zhang, C. Fuentes-Hernandez, S. Barlow, S. R. Marder and B. Kippelen, Host-free yellow-green organic light-emitting diodes with external quantum efficiency over 20% based on a compound exhibiting thermally activated delayed fluorescence, *ACS Appl. Mater. Interfaces* **2019**, *11*, 12693.

[38]. N. B. Kotadiya, P. W. M. Blom, G.-J. A. H. Wetzelaer, Efficient and stable single-layer organic light-emitting diodes based on thermally activated delayed fluorescence, *Nat. Photonics* **2019**, DOI: 10.1038/s41566-019-0488-1.

[39]. X. Q. Zhang, C. Fuentes-Hernandez, Y. D. Zhang, M. W. Cooper, S. Barlow, S. R. Marder and B. Kippelen, High performance blue-emitting organic light-emitting diodes from thermally activated delayed fluorescence: A guest/host ratio study, *J. Appl. Phys.* **2018**, *124*, 055501.

[40]. T. Y. Huang, W. Jiang and L. Duan, Recent progress in solution processable TADF materials for organic light-emitting diodes, *J. Mater. Chem. C* **2018**, *6*, 5577.

[41]. X. L. Chen, J. H. Jia, R. Yu, J. Z. Liao, M. X. Yang and C. Z. Lu, Combining charge-transfer pathways to achieve unique thermally activated delayed fluorescence emitters for

high-performance solution-processed, non-doped blue OLEDs, *Angew. Chem. Int. Ed. Engl*. **2017**, *56*, 15006.
[42]. M. Godumala, S. Choi, M. J. Cho and D. H. Choi, Recent breakthroughs in thermally activated delayed fluorescence organic light emitting diodes containing non-doped emitting layers, *J. Mater. Chem. C* **2019**, *7*, 2172.
[43]. C. C. Wu, Y. T. Lin, K. T. Wong, R. T. Chen and Y. Y. Chien, Efficient organic blue-light-emitting devices with double confinement on terfluorenes with ambipolar carrier transport properties, *Adv. Mater.* **2004**, *16*, 61.
[44]. K. Albrecht, K. Matsuoka, K. Fujita and K. Yamamoto, Carbazole dendrimers as solution-processable thermally activated delayed-fluorescence materials, *Angew. Chem. Int. Ed. Engl*. **2015**, *127*, 5769.
[45]. A. R. G. Smith, J. L. Ruggles, H. Cavaye, P. E. Shaw, T. A. Darwish, M. James, I. R. Gentle and P. L. Burn, Investigating morphology and stability of fac-tris (2-phenylpyridyl)iridium(III) films for OLEDs, *Adv. Funct. Mater.*, **2011**, *21*, 2225.
[46]. L. H. Liu, X. J. Liu, K. Q. Wu, J. Q. Ding, B. H. Zhang, Z. Y. Xie and L. X. Wang, Efficient solution-processed blue phosphorescent organic light-emitting diodes with halogen-free solvent to optimize the emissive layer morphology, *Org. Electron.*, **2014**, *15*, 1401.
[47]. R. X. Huang, I. Chavez, K. M. Taute, B. Lukic, S. Jeney, M. G. Raizen and E. L. Florin, Direct observation of the full transition from ballistic to diffusive Brownian motion in a liquid, *Nat. Phys.*, **2011**, *7*, 576.
[48]. E. Skuodis, O. Bezvikonnyi, A. Tomkeviciene, D. Volyniuk, V. Mimaite, A. Lazauskas, A. Bucinskas, R. Keruckiene, G. Sini and J. V. Grazulevicius, Aggregation, thermal annealing, and hosting effects on performances of an acridan-based TADF emitter, *Org. Electron.* **2018**, *63*, 29.
[49]. S. Burns, J. MacLeod, T. T. Do, P. Sonar and S. D. Yambem, Effect of thermal annealing Super Yellow emissive layer on efficiency of OLEDs, *Sci. Rep.* **2017**, *7*, 40805.
[50]. T. B. de Queiroz and S. Kummel, Tuned range separated hybrid functionals for solvated low bandgap oligomers, *J. Chem. Phys.* **2015**, *143*, 034101.
[51]. L. Kronik and S. Kummel, Dielectric screening meets optimally tuned density functionals*, Adv. Mater.* **2018***, 30,* 1706560.
[52]. Y. Olivier, B. Yurash, L. Muccioli, G. D'Avino, O. Mikhnenko, J. C. Sancho-Garcia, C. Adachi, T. Q. Nguyen and D. Beljonne, Nature of the singlet and triplet excitations mediating thermally activated delayed fluorescence, *Phy. Rev. Mater.* **2017**, *1*, 075602.
[53]. Y. Olivier, J. C. Sancho-Garcia, L. Muccioh, G. D'Avino and D. Beljonne, Computational design of thermally activated delayed fluorescence materials: the challenges ahead, *J. Phys. Chem. Lett.* **2018**, *9*, 6149.
[54]. J. Mei, Y. Hong, J. W. Y. Lam, A. Qin, Y. Tang and B. Z. Tang, Aggregation-induced emission: the whole is more brilliant than the parts, *Adv. Mater.* **2014**, *26*, 5429.
[55]. V. Jankus, P. Data, D. Graves, C. McGuinness, J. Santos, M. R. Bryce, F. B. Dias and A. P. Monkman, Highly efficient TADF OLEDs: how the emitter–host interaction controls both the excited state species and electrical properties of the devices to achieve near 100% triplet harvesting and high efficiency, *Adv. Funct. Mater.* **2014**, *24*, 6178.
[56]. D. Virgili, M. Cocchi, V. Fattori, C. Sabatini, J. Kalinowski and J. A. G. Williams, Highly efficient exciplex phosphorescence from organic light-emitting diodes, *Chem. Phys. Lett.* **2006**, *433*, 145.

[57]. D. M. Sun, Z. J. Ren, M. R. Bryce and S. K. Yan, Arylsilanes and siloxanes as optoelectronic materials for organic light-emitting diodes (OLEDs), *J. Mater. Chem. C* **2015**, *3*, 9496.
[58]. X. Wang, S. Wang, J. Lv, S. Shao, L. Wang, X. Jing and F. Wang, Through-space charge transfer hexaarylbenzene dendrimers with thermally activated delayed fluorescence and aggregation-induced emission for efficient solution-processed OLEDs, *Chem. Sci.* **2019**, *10*, 2915.
[59]. R. C. Hilborn, Einstein coefficients, cross-sections, *f* values, dipole-moments, and all that, *Am. J. Phys.* **1982**, *50*, 982.
[60]. R. A. Marcus, Electron-transfer reactions in chemistry-theory and experiment, *Rev. Mod. Phys.* **1993**, *65*, 599.
[61]. P. K. Samanta, D. Kim, V. Coropceanu and J.-L. Brédas, Up-conversion intersystem crossing rates in organic emitters for thermally activated delayed fluorescence: impact of the nature of singlet vs triplet excited states, *J. Am. Chem. Soc.* **2017**, *139*, 4042.
[62]. K. Masui, H. Nakanotani and C. Adachi, Analysis of exciton annihilation in high-efficiency sky-blue organic light-emitting diodes with thermally activated delayed fluorescence, *Org. Electron.*, **2013**, *14*, 2721.
[63]. S. Scholz, D. Kondakov, B. Lussem and K. Leo, Degradation mechanisms and reactions in organic light-emitting devices, *Chem. Rev.*, **2015**, *115*, 8449.
[64]. V. Russo, C. Curutchet and B. Mennucci, Towards a molecular scale interpretation of excitation energy transfer in solvated bichromophoric systems. II. The through-bond contribution, *J. Phys. Chem. B* **2007**, *111*, 853.
[65]. C. Curutchet and B. Mennucci, Toward a molecular scale interpretation of excitation energy transfer in solvated bichromophoric systems, *J. Am. Chem. Soc*. **2005**, *127*, 16733.
[66]. S. R. Scully, P. B. Armstrong, C. Edder, J. M. J. Frechet and M. D. McGehee, Long-range resonant energy transfer for enhanced exciton harvesting for organic solar cells, *Adv. Mater.* **2007**, *19*, 2961.
[67]. E. B. Namdas, A. Ruseckas, I. D. W. Samuel, S. C. Lo and P. L. Burn, Triplet exciton diffusion in fac-tris(2-phenylpyridine) iridium(III)-cored electroluminescent dendrimers, *Appl. Phys. Lett.* **2005**, 86, 091104.
[68]. O. V. Mikhnenko, M. Kuik, J. Lin, N. van der Kaap, T. Q. Nguyen and P. W. M. Blom, Trap- limited exciton diffusion in organic semiconductors, *Adv. Mater.* **2014**, *26*, 1912.
[69]. W. A. Luhman and R. J. Holmes, Investigation of energy transfer in organic photovoltaic cells and impact on exciton diffusion length measurements, *Adv. Funct. Mater.* **2011**, *21*, 764.
[70]. N. C. Giebink, Y. Sun and S. R. Forrest, Transient analysis of triplet exciton dynamics in amorphous organic semiconductor thin films, *Org. Electron.* **2006**, *7*, 375.
[71]. K. Feron, W. J. Belcher, C. J. Fell and P. C. Dastoor, Organic solar cells: understanding the role of forster resonance energy transfer, *Int. J Mol. Sci.* **2012**, *13*, 17019.
[72]. S. M. Menke and R. J. Holmes, Exciton transport in an organic semiconductor exhibiting thermally activateddelayed fluorescence, *J. Phys. Chem. C* **2016**, *120*, 8502.
[73]. O. V. Mikhnenko, P. W. M. Blom and T. Q. Nguyen, Exciton diffusion in organic semiconductors, *Energ Environ. Sci*. **2015**, *8*, 1867.
[74]. R. R. Lunt, N. C. Giebink, A. A. Belak, J. B. Benziger and S. R. Forrest, Exciton diffusion lengths of organic semiconductor thin films measured by spectrally resolved photoluminescence quenching, *J. Appl. Phys.*, **2009**, *105*.

[75]. T. Forster, Zwischenmolekulare Energiewanderung Und Fluoreszenz, *Annalen Der Physik* **1948**, *2*, 55.
[76]. J. Lee, N. Aizawa, M. Numata, C. Adachi and T. Yasuda, Versatile molecular functionalization for inhibiting concentration quenching of thermally activated delayed fluorescence, *Adv. Mater.* **2017**, *29*, 1604856.
[77]. D. L. Dexter, A theory of sensitized luminescence in solids, *J. Chem. Phys.* **1953**, *21*, 836.
[78]. H. S. Kim, S. R. Park and M. C. Suh, Concentration quenching behavior of thermally activated delayed fluorescence in a solid Film, *J. Phys. Chem. C* **2017**, *121*, 13986.
[79]. X.-K. Chen, B. W. Bakr, M. Auffray, Y. Tsuchiya, C. D. Sherrill, C. Adachi and J.-L. Bredas, Intramolecular noncovalent interactions facilitate thermally activated delayed fluorescence (TADF), *J. Phys. Chem. Lett.* **2019**, *10*, 3260.
[80]. J. C. Phillips, R. Braun, W. Wang, J. Gumbart, E. Tajkhorshid, E. Villa, C. Chipot, R. D. Skeel, L. Kale and K. Schulten, Scalable molecular dynamics with NAMD, *J. Comput. Chem.* **2005**, *26*, 1781.
[81]. S. E. Feller, Y. H. Zhang, R. W. Pastor and B. R. Brooks, Constant-pressure molecular-dynamics simulation - the langevin piston method, *J. Chem. Phys.* **1995**, *103*, 4613.
[82]. T. Darden, D. York and L. Pedersen, Particle mesh ewald - an N.Log(N) method for ewald sums in large systems, *J. Chem. Phys.* **1993**, *98*, 10089.
[83]. W. L. Jorgensen, D. S. Maxwell and J. TiradoRives, Development and testing of the OPLS all-atom force field on conformational energetics and properties of organic liquids, *J. Am. Chem. Soc.* **1996**, *118*, 11225.
[84]. K. Do, M. K. Ravva, T. H. Wang and J. L. Bredas, Computational methodologies for developing structure-morphology-performance relationships in organic solar cells: a protocol review, *Chem. Mater.* **2017**, *29*, 346.
[85]. Gaussian 16, Revision A.03, M. J. Frisch, G. W. Trucks, H. B. Schlegel, G. E. Scuseria, M. A. Robb, J. R. Cheeseman, G. Scalmani, V. Barone, G. A. Petersson, H. Nakatsuji, X. Li, M. Caricato, A. V. Marenich, J. Bloino, B. G. Janesko, R. Gomperts, B. Mennucci, H. P. Hratchian, J. V. Ortiz, A. F. Izmaylov, J. L. Sonnenberg, Williams, F. Ding, F. Lipparini, F. Egidi, J. Goings, B. Peng, A. Petrone, T. Henderson, D. Ranasinghe, V. G. Zakrzewski, J. Gao, N. Rega, G. Zheng, W. Liang, M. Hada, M. Ehara, K. Toyota, R. Fukuda, J. Hasegawa, M. Ishida, T. Nakajima, Y. Honda, O. Kitao, H. Nakai, T. Vreven, K. Throssell, J. A. Montgomery Jr., J. E. Peralta, F. Ogliaro, M. J. Bearpark, J. J. Heyd, E. N. Brothers, K. N. Kudin, V. N. Staroverov, T. A. Keith, R. Kobayashi, J. Normand, K. Raghavachari, A. P. Rendell, J. C. Burant, S. S. Iyengar, J. Tomasi, M. Cossi, J. M. Millam, M. Klene, C. Adamo, R. Cammi, J. W. Ochterski, R. L. Martin, K. Morokuma, O. Farkas, J. B. Foresman and D. J. Fox, Gaussian, Inc., Wallingford CT, **2016**.
[86]. J. D. Chai and M. Head-Gordon, Long-range corrected hybrid density functionals with damped atom-atom dispersion corrections, *Phys. Chem. Chem. Phys.* **2008**, *10*, 6615.
[87]. L. Kronik, T. Stein, S. Refaely-Abramson and R. Baer, Excitation gaps of finite-sized systems from optimally tuned range-separated hybrid functionals, *J. Chem. Theory. Comput.* **2012**, *8*, 1515.
[88]. Y. Jiang, Z. Hu, B. Zhou, C. Zhong, Z. Sun and H. Sun, Accurate prediction for dynamic hybrid local and charge transfer excited states from optimally tuned range-separated density functionals, *J. Phys. Chem. C* **2019**, *123*, 5616.

[89]. T. Hu, G. Han, Z. Tu, R. Duan and Y. Yi, Origin of high efficiencies for thermally activated delayed fluorescence organic light-emitting diodes: atomistic insight into molecular orientation and torsional disorder, *J. Phys. Chem. C* **2018**, *122*, 27191.
[90]. H. Sun, Z. Hu, C. Zhong, X. Chen, Z. Sun and J.-L. Brédas, Impact of dielectric constant on the singlet–triplet gap in thermally activated delayed fluorescence materials, *J. Phys. Chem. Lett.* **2017**, *8*, 2393.
[91]. S. Hirata and M. Head-Gordon, Time-dependent density functional theory within the Tamm-Dancoff approximation, *Chem. Phys. Lett.* **1999**, *314*, 291.
[92]. C. P. Hsu, S. Hirata and M. Head-Gordon, Excitation energies from time-dependent density functional theory for linear polyene oligomers: Butadiene to decapentaene, *J. Phys. Chem. A* **2001**, *105*, 451.
[93]. Y. L. Wang and G. S. Wu, Improving the TDDFT calculation of low-lying excited states for polycyclic aromatic hydrocarbons using the Tamm-Dancoff approximation, *Int. J. Quantum Chem.* **2008**, *108*, 430.
[94]. S. Hirata and M. Head-Gordon, Time-dependent density functional theory for radicals - An improved description of excited states with substantial double excitation character, *Chem. Phys. Lett.* **1999**, *302*, 375.
[95]. H. Sun, C. Zhong, and J. L. Bredas, Reliable prediction with tuned range-separated functionals of the singlet-triplet gap in organic emitters for thermally activated delayed fluorescence, *J. Chem. Theory Comput.* **2015**, *11*, 3851.
[96]. M. J. Peach, and D. J. Tozer, Overcoming low orbital overlap and triplet instability problems in TDDFT, *J. Phys. Chem. A* **2012**, *116*, 9783.
[97]. X. Gao, S. M. Bai, D. Fazzi, T. Niehaus, M. Barbatti and W. Thiel, Evaluation of spin-orbit couplings with linear-response time-dependent density functional methods, *J. Chem. Theory. Comput.* **2017**, *13*, 515.
[98]. S. G. Chiodo and M. Leopoldini, MoISOC: A spin-orbit coupling code, *Comput. Phys. Commun.* **2014**, *185*, 676.
[99]. D. Toptygin, Effects of the solvent refractive index and its dispersion on the radiative decay rate and extinction coefficient of a fluorescent solute, *J. Fluoresc.* **2003**, *13*, 201.
[100]. Z.-Q. You and C.-P. Hsu, Theory and calculation for the electronic coupling in excitation energy transfer, *Int. J. Quantum. Chem*. 2014, 114, 102.
[101]. B. P. Krueger, G. D. Scholes and G. R. Fleming, Calculation of couplings and energy-transfer pathways between the pigments of LH2 by the ab initio transition density cube method, *J. Phys. Chem. B* **1998**, *102*, 5378.
[102]. C. P. Hsu, G. R. Fleming, M. Head-Gordon and T. Head-Gordon, Excitation energy transfer in condensed media, *J. Chem. Phys.* **2001**, *114*, 3065.
[103]. J. A. Freund and T. Pöschel, *Stochastic processes in physics, chemistry, and biology*, Springer, Berlin **2000**.
[104]. M. Pope and C. E. Swenberg, *Electronic processes in organic crystals and polymers*, Oxford University Press, New York **1999**.
[105]. V. Coropceanu, J. Cornil, D. A. da Silva, Y. Olivier, R. Silbey and J. L. Bredas, Charge transport in organic semiconductors, *Chem. Rev.* **2007**, *107*, 926.